POLITECNICO DI TORINO
Repository ISTITUZIONALE

Microscopic theory of vertical-transport phenomena in semiconductor heterostructures: Interplay between two- and three-dimensional hot-carrier relaxation

*Original*
Microscopic theory of vertical-transport phenomena in semiconductor heterostructures: Interplay between two- and three-dimensional hot-carrier relaxation / Barbieri, S.; Beltram, F.; Rossi, Fausto. - In: PHYSICAL REVIEW. B, CONDENSED MATTER AND MATERIALS PHYSICS. - ISSN 1098-0121. - 60:3(1999), pp. 1953-1963. [10.1103/PhysRevB.60.1953]

*Availability:*
This version is available at: 11583/1405211 since: 2016-09-13T11:49:17Z

*Publisher:*
APS The Americal Physical Society

*Published*
DOI:10.1103/PhysRevB.60.1953

*Terms of use:*

This article is made available under terms and conditions as specified in the corresponding bibliographic description in the repository

*Publisher copyright*

(Article begins on next page)

21 December 2024

# Microscopic theory of vertical-transport phenomena in semiconductor heterostructures: Interplay between two- and three-dimensional hot-carrier relaxation

Stefano Barbieri and Fabio Beltram
*Scuola Normale Superiore and Istituto Nazionale per la Fisica della Materia (INFM), Piazza dei Cavalieri 7, 56126 Pisa, Italy*

Fausto Rossi
*INFM and Dipartimento di Fisica, Politecnico di Torino, Corso Duca degli Abruzzi 24, 10129 Torino, Italy*
(Received 12 October 1998)

A theoretical analysis of vertical-transport phenomena in semiconductor heterostructures is presented. In particular, the scattering coupling between two- and three-dimensional states in multiple quantum wells is investigated. To this purpose, a fully three-dimensional approach for the description of both localized and extended states in the heterostructure is proposed. Starting from such three-dimensional states, obtained from a self-consistent Schrödinger-Poisson calculation, a Monte Carlo solution of the corresponding Boltzmann transport equation is performed. In contrast to various phenomenological transport models, the present simulation scheme allows a kinetic description, i.e., based on microscopic scattering rates, of vertical transport across a generic heterostructure. Our results provide a rigorous description of hot-carrier relaxation between extended and localized states. This simulation scheme has been applied to finite multiple quantum wells with different geometries and doping profiles. A detailed analysis of the electron current as a function of temperature in quasiequilibrium conditions shows good agreement with experimental results. Moreover, in nonequilibrium conditions (i.e., hot-carrier regime) the scattering coupling between three- and two-dimensional states is found to play a significant role in modifying the carrier mobility as well as the fraction of conducting electrons. [S0163-1829(99)00924-8]

## I. INTRODUCTION

Semiconductor heterostructures[1] have been the subject of an impressive research activity,[2–4] owing to their great flexibility as model systems for basic research as well as effective ''building blocks'' in modern solid-state optoelectronic devices. For the case of periodic heterostructures in particular, among the most successful applications one must mention a variety of photodetectors, i.e., avalanche photodetectors,[5] far-infrared detectors,[6,7] and, more recently, hot-carrier photodetectors operating in the microwave range.[8,9]

The principle of operation for most of these solid-state devices involves nonequilibrium carrier dynamics between propagating and localized states in the heterostructure,[10–12] i.e., ionization vs capture processes. This dynamics is strongly influenced by phonon scattering as well as by carrier concentration and temperature.

The most commonly used approach for the theoretical analysis of energy-relaxation[3] and transport experiments[4] is the Monte Carlo method,[13–15] both in bulk and in low-dimensional structures. This has proven to be a very powerful technique, allowing the inclusion at a kinetic level of a large variety of scattering processes (carrier-phonon, carrier-carrier, carrier-plasmon, inter-valence band, intervalley, etc.). The role of these scattering processes, in turn, is influenced by the choice of the experimental conditions. For instance, carrier-carrier scattering and hot-phonon effects strongly depend on the density, and intervalley transitions are suppressed if the excitation is below the threshold for this process. Thus the combination of direct measurements and ''simulated experiments'' provides detailed information on the relevant scattering rates and coupling constants.

The theoretical investigation of carrier transport in heterostructures proposed so far, however, was always limited to Monte Carlo simulations of systems with a well-defined dimensionality, i.e., no interplay between propagating and localized states was treated at a fully microscopic level. While the carrier dynamics within a given structure, e.g., a quantum-well (QW) laser, is usually modeled in terms of the corresponding Boltzmann equation, its coupling with the three-dimensional continuum is typically described in terms of purely phenomenological ionization/capture times.

In this paper, we present a microscopic theory of vertical-transport phenomena in semiconductor heterostructures. The aim is to investigate the scattering dynamics between two- and three-dimensional (2D and 3D) states in multiple quantum wells (MQW's). To this end, a fully 3D approach for the description of both localized and extended states in the heterostructure is proposed. Single-particle states are obtained from a self-consistent Schrödinger-Poisson calculation within a plane-wave representation, and are exploited to derive a set of Boltzmann-like kinetic equations describing vertical transport across a generic heterostructure in the presence of carrier-phonon scattering. Our numerical approach is based on a Monte Carlo solution of this set of coupled equations within a multiminiband scheme. It can be regarded as a generalization to heterostructures of the Monte Carlo simulation proposed in Ref. 16 for the analysis of Bloch oscillations in semiconductor superlattices (SL's).

Compared to various phenomenological transport models,[6,7,11,17–19] the present simulation scheme allows a kinetic description, i.e., based on microscopic scattering rates, of transport phenomena, thus providing a rigorous descrip-

 ©1999 The American Physical Society

tion of hot-carrier relaxation between extended (3D-like) and localized (2D-like) states.

The above simulation scheme has been applied to finite MQW's with different geometries and doping profiles. A detailed investigation of the electron current as a function of temperature in quasiequilibrium conditions shows a good agreement with experimental results. Moreover, for nonequilibrium conditions, i.e., the hot-carrier regime, the phonon-induced scattering between 3D and 2D states is found to play a significant role in modifying the carrier mobility as well as the actual fraction of conducting electrons.

The paper is organized as follows: In Sec. II we introduce the physical system, the theoretical approach, and the weighted Monte Carlo procedure used for the solution of our set of Boltzmann transport equations. In Sec. III the results of our ''simulated experiments'' are presented and compared with available transport measurements. Finally, in Sec. IV, we shall summarize and draw some conclusions.

## II. THEORETICAL APPROACH

### A. Physical system

The physical system under investigation is a gas of carriers confined in a quasi-2D semiconductor heterostructure. As usual, the total Hamiltonian of the system can be regarded as the sum of two terms:

$$\mathbf{H}=\mathbf{H}_0+\mathbf{H}'. \tag{1}$$

The first term describes single-particle properties, e.g., free carriers and phonons plus heterostructure potential profile plus applied field; the second term describes many-body effects, e.g., carrier-phonon interaction.

Quantum confinement induced by the heterostructure is described in terms of a potential profile $V_0(z)$ ($z$ being the growth direction) whose value is dictated by the conduction-band discontinuities. Since the energy region of interest is relatively close to the semiconductor band gap, we describe the bulk band structure in terms of the usual effective-mass approximation. Moreover, we describe the electronic states in the heterostructure within the well-known envelope-function picture. As a consequence, the full 3D carrier wave function can be factorized in terms of a 2D plane wave times a one-dimensional envelope function along the growth direction,

$$\psi(\mathbf{r})=e^{i\mathbf{k}_\parallel\cdot\mathbf{r}_\parallel}\phi(z), \tag{2}$$

where $\mathbf{k}_\parallel$ is the in-plane component of the carrier wave vector.

Moreover, in order to describe a large variety of heterostructures, i.e., ranging from single- or double-well structures to infinite SL's, we employ a periodic-boundary-condition scheme along the growth direction. This corresponds to writing the carrier wave function $\phi(z)$ as

$$\phi_{k_z}(z)=e^{ik_z z}u_{k_z}(z), \tag{3}$$

where the periodic function $u$ (over one period length, $L_z$) has been introduced: $u_{k_z}(z)=u_{k_z}(z+L_z)$.

Since our interest is mainly devoted to unipolar vertical transport, most of the relevant structures are characterized by relatively high doping concentrations. Thus the solution of the 1D Schrödinger equation for $\phi_{k_z}(z)$ has to be performed self-consistently with that of the corresponding Poisson equation. Our numerical approach to this self-consistent solution is described in Appendix A; it is based on a plane-wave expansion of both equations with periodic boundary conditions. Compared to more conventional Schrödinger-Poisson calculations in real-space coordinates, the use of a full plane-wave description for the self-consistent solution of both equations is rather stable and efficient.

The single-particle Hamiltonian in Eq. (1) can be schematically written as

$$\mathbf{H}_0=\mathbf{H}_c+\mathbf{H}_\mathbf{F}+\mathbf{H}_p. \tag{4}$$

More specifically,

$$\mathbf{H}_c=\sum_{\mathbf{k}\nu}\mathcal{E}_{\mathbf{k}\nu}a^\dagger_{\mathbf{k}\nu}a_{\mathbf{k}\nu} \tag{5}$$

is the free-carrier Hamiltonian written in the usual second-quantization picture. Here $\mathbf{k}=(\mathbf{k}_\parallel,k_z)$ and $\nu$ denote, respectively, the 3D carrier wave vector and miniband index, while $a^\dagger_{\mathbf{k}\nu}$ and $a_{\mathbf{k}\nu}$ are creation and destruction operators of electrons with wave vector $\mathbf{k}$ in miniband $\nu$. $\mathcal{E}_{\mathbf{k}\nu}$ is the 3D electron energy band:

$$\mathcal{E}_{\mathbf{k}\nu}=\epsilon_{k_z\nu}+\frac{\hbar^2k_\parallel^2}{2m_\parallel}. \tag{6}$$

For each 1D miniband level $\epsilon_{k_z\nu}$, we thus have a 2D parabolic subband characterized by an effective mass $m_\parallel$.

The term

$$\mathbf{H}_\mathbf{F}=\sum_{\mathbf{k}\nu,\mathbf{k}'\nu'}\alpha_{\mathbf{k}\nu,\mathbf{k}'\nu'}a^\dagger_{\mathbf{k}\nu}a_{\mathbf{k}'\nu'} \tag{7}$$

describes the effect of a uniform applied electric field $\mathbf{F}$; the quantities $\alpha_{\mathbf{k}\nu,\mathbf{k}'\nu'}$ denote the matrix elements of the corresponding scalar potential $-e\mathbf{F}\cdot\mathbf{r}$ in our $\mathbf{k}\nu$ representation.

The term

$$\mathbf{H}_p=\sum_{\mathbf{q}}\hbar\omega_\mathbf{q}b^\dagger_\mathbf{q}b_\mathbf{q} \tag{8}$$

describes the free-phonon dynamics. As usual, $b^\dagger_\mathbf{q}(b_\mathbf{q})$ denote the creation (annihilation) operators of phonons with wave vector $\mathbf{q}$, while $\omega_\mathbf{q}$ is the phonon dispersion. For simplicity, we consider a single-phonon mode; the generalization, if necessary, is obvious.

For what concerns the last contribution in Eq. (1), in this paper we shall consider exclusively the dominant contribution due to carrier-phonon interaction:

$$\mathbf{H}'=\sum_{\mathbf{k}\nu,\mathbf{k}'\nu';\mathbf{q}}[g_{\mathbf{k}\nu,\mathbf{k}'\nu';\mathbf{q}}a^{\dagger}_{\mathbf{k}\nu}b^{\dagger}_{\mathbf{q}}a_{\mathbf{k}'\nu'}+g^{*}_{\mathbf{k}\nu,\mathbf{k}'\nu';\mathbf{q}}a^{\dagger}_{\mathbf{k}'\nu'}b_{\mathbf{q}}a_{\mathbf{k}\nu}]. \tag{9}$$

Here, the quantities $g$ denote the matrix elements of the phonon electrostatic potential in the $\mathbf{k}\nu$ representation. As we shall see, the above Hamiltonian describes both intraminiband ($\nu=\nu'$) and interminiband ($\nu\neq\nu'$) carrier-phonon scattering processes.

In this paper we shall describe the phonon system in terms of a single GaAs bulk LO-phonon mode. In this case, the matrix elements $g$ are given by

$$g_{\mathbf{k}\nu,\mathbf{k}'\nu';\mathbf{q}}=\tilde{g}_{\mathbf{q}}\int d\mathbf{r}\,\psi^{*}_{\mathbf{k}'\nu'}(\mathbf{r})e^{i\mathbf{q}\cdot\mathbf{r}}\psi_{\mathbf{k}\nu}(\mathbf{r}), \tag{10}$$

where

$$\tilde{g}_{\mathbf{q}}=g_0\frac{1}{q}=\left[\frac{2\pi e^2\hbar\omega_0}{\Omega}\left(\frac{1}{\varepsilon_\infty}-\frac{1}{\varepsilon_0}\right)\right]^{1/2}\frac{1}{q} \tag{11}$$

is the coupling constant for the Fröhlich interaction with dispersionless bulk LO phonons of energy $\hbar\omega_0$. Here $\varepsilon_\infty$ and $\varepsilon_0$ denote the optical and static dielectric constants of the ''effective'' medium, and $\Omega$ is the 3D normalization volume.

This simplifying approximation neglects any heterostructure effect on the phonon dispersion, such as confinement of optical modes in the wells and in the barriers, and the presence of interface modes.[20] However, while these modifications have important consequences for phonon spectroscopy (e.g., Raman scattering), they are far less decisive for transport phenomena. Indeed, by now it is well known[20,21] that the total scattering rates are sufficiently well reproduced if the phonon spectrum is assumed to be bulklike.

### B. Kinetic description

Let us now introduce the set of kinetic variables used to describe the carrier system within our semiconductor heterostructure. We choose the various carrier distribution functions corresponding to the different conduction minibands:

$$f_{\mathbf{k}\nu}=\langle a^{\dagger}_{\mathbf{k}\nu}a_{\mathbf{k}\nu}\rangle. \tag{12}$$

As usual these distribution functions correspond to the diagonal elements ($\mathbf{k}\nu=\mathbf{k}'\nu'$) of the single-particle density matrix. These are the only kinetic variables of interest in the present work since we shall not consider coherent interband phenomena which play a significant role only in determining the ultrafast dynamics of photoexcited carriers.[22,23]

Let us now discuss the time evolution of these kinetic variables in terms of their dynamic equations:

$$\frac{d}{dt}f_{\mathbf{k}\nu}=\frac{1}{i\hbar}\langle[a^{\dagger}_{\mathbf{k}\nu}a_{\mathbf{k}\nu},\mathbf{H}]\rangle. \tag{13}$$

According to the separation $\mathbf{H}=\mathbf{H}_0+\mathbf{H}'$ in Eq. (1), we can identify two contributions in the equations of motion of the distribution functions:

$$\frac{d}{dt}f_{\mathbf{k}\nu}=\left.\frac{d}{dt}f_{\mathbf{k}\nu}\right|_{\mathbf{H}_0}+\left.\frac{d}{dt}f_{\mathbf{k}\nu}\right|_{cp}. \tag{14}$$

By neglecting interminiband terms in Eq. (7) the time evolution induced by the Hamiltonian $\mathbf{H}_0$ can be evaluated exactly[24]:

$$\left.\frac{d}{dt}f_{\mathbf{k}\nu}\right|_{\mathbf{H}_0}=-\dot{\mathbf{k}}\cdot\nabla_{\mathbf{k}}f_{\mathbf{k}\nu}=-\frac{e\mathbf{F}}{\hbar}\cdot\nabla_{\mathbf{k}}f_{\mathbf{k}\nu}. \tag{15}$$

This is the well-known drift term in the Boltzmann transport theory,[15] which in the present context describes the carrier acceleration within each miniband induced by the applied electric field $\mathbf{F}$.

The second term on the right-hand side of Eq. (14)—induced by the carrier-phonon Hamiltonian (9)—cannot be treated exactly within our kinetic description. Here we shall employ the standard semiclassical approximation (i.e., mean field plus Markov limit), and we shall not discuss the details of the derivation which is similar to that of Ref. 22 for the case of a bulk semiconductor. Within such an approximation scheme, a Markov limit is performed, and therefore various memory and intracollisional field effects are neglected. However, the vertical-transport phenomena discussed in this paper—induced by moderate electric fields—are not sensitive to such effects.

Within this semiclassical approximation the carrier-phonon contribution in Eq. (14) is given by the rate equation

$$\left.\frac{d}{dt}f_{\mathbf{k}\nu}\right|_{cp}=\sum_{\mathbf{k}'\nu'}[P_{\mathbf{k}\nu,\mathbf{k}'\nu'}f_{\mathbf{k}'\nu'}-P_{\mathbf{k}'\nu',\mathbf{k}\nu}f_{\mathbf{k}\nu}], \tag{16}$$

where $P_{\mathbf{k}\nu,\mathbf{k}'\nu'}$ is the carrier-phonon scattering probability for a transition from state $\mathbf{k}\nu$ to state $\mathbf{k}'\nu'$. It is easy to recognize the typical structure of the ''Boltzmann collision term,'' i.e., an in-scattering contribution plus an out-scattering contribution.[13,15] Within our semiclassical approach, the explicit form of these scattering probabilities is given by

$$P_{\mathbf{k}\nu,\mathbf{k}'\nu'}=\sum_{\pm}\frac{2\pi}{\hbar}\sum_{\mathbf{q}}|g_{\mathbf{k}'\nu',\mathbf{k}\nu;\pm\mathbf{q}}|^2\left(N_{\mathbf{q}}+\frac{1}{2}\mp\frac{1}{2}\right)(1-f_{\mathbf{k}'\nu'})\,\delta(\mathcal{E}_{\mathbf{k}'\nu'}-\mathcal{E}_{\mathbf{k}\nu}\pm\hbar\omega_{\mathbf{q}}), \tag{17}$$

where $N_{\mathbf{q}}$ is the phonon occupation number and the upper (lower) sign refers to phonon absorption (emission).

By inserting the explicit form of the various contributions into Eq. (14), we can finally write down the set of coupled Boltzmann equations which govern carrier transport in our semiconductor heterostructure:

$$\frac{\partial}{\partial t}f_{\mathbf{k}\nu}+\frac{e\mathbf{F}}{\hbar}\cdot\nabla_{\mathbf{k}}f_{\mathbf{k}\nu}=\sum_{\mathbf{k}'\nu'}[P_{\mathbf{k}\nu,\mathbf{k}'\nu'}f_{\mathbf{k}'\nu'}-P_{\mathbf{k}'\nu',\mathbf{k}\nu}f_{\mathbf{k}\nu}]. \tag{18}$$

### C. Weighted Monte Carlo procedure

As discussed in Sec. II B, the carrier dynamics in our semiconductor heterostructure is described in terms of the coupled set of Boltzmann-like equations (18) for the various distribution functions $f_{\mathbf{k}\nu}$ in the different minibands. It can be schematically written as

$$\frac{\partial}{\partial t}f_{\mathbf{k}\nu}+\frac{e\mathbf{F}}{\hbar}\cdot\nabla_{\mathbf{k}}f_{\mathbf{k}\nu}=\left.\frac{d}{dt}f_{\mathbf{k}\nu}\right|_{cp}. \tag{19}$$

Following the approach described in Ref. 15, we can introduce a coordinate transformation to a new set of variables called ''path variables'':

$$\tilde{\mathbf{k}}=\mathbf{k}-\dot{\mathbf{k}}(t-t_0), \tag{20}$$

with $\dot{\mathbf{k}}=e\mathbf{F}/\hbar$, and a corresponding transformed distribution function $\tilde{f}$ defined by

$$\tilde{f}_{\tilde{\mathbf{k}}\nu}=f_{\mathbf{k}\nu}. \tag{21}$$

This transformation eliminates the drift term on the left-hand side of Eq. (19), which can now be rewritten

$$\frac{d}{dt}\tilde{f}_{\tilde{\mathbf{k}}\nu}=\left.\frac{d}{dt}\tilde{f}_{\tilde{\mathbf{k}}\nu}\right|_{cp}. \tag{22}$$

The acceleration induced by the applied electric field, previously described by the drift term, is now implicitly contained in $\tilde{\mathbf{k}}$, i.e., $\tilde{\mathbf{k}}$ is a function of time [see Eq. (20)]. In the absence of carrier-phonon scattering, the transformed distribution function $\tilde{f}$ is constant in time, and thus from Eq. (21) we obtain:

$$f_{\mathbf{k}\nu}(t)=f_{\mathbf{k}-\dot{\mathbf{k}}(t-t_0),\nu}(t_0). \tag{23}$$

Following the spirit of the number representation introduced in Ref. 22 for the bulk case, we employ a suitable $\mathbf{k}$-space discretization similar to that used in Ref. 16 for the study of Bloch oscillations in SL's. In particular, due to the symmetry of our system, we define a cylindrical (two-dimensional) grid, and for each cell of the grid we introduce an integer number $n_{i\nu}$ which denotes the number of carriers in the $i$-th cell and miniband $\nu$.

Due to the dependence of the scattering rates on the distribution functions [see Eq. (17)], the set of kinetic equations (22) is nonlinear and, therefore, we are forced to perform a time-step solution. In particular, we employ a fixed time-step $\Delta t$ over which our kinetic equations are locally linear and decoupled.[22]

Schematically our total simulation time is divided into a sequence of time-steps. For each of them the following are true.

(i) A random sequence of free flights and scattering events is generated for each carrier in the various minibands. The result is a random walk both over $\mathbf{k}$ and over the different minibands.

(ii) The carrier distributions $f_{\mathbf{k}\nu}$ (i.e., the occupation numbers $n_{i\nu}$ over our $\mathbf{k}$-space grid) are updated at the end of the time-step.

As we shall see, for most of the hot-carrier phenomena discussed in this paper the fraction of carriers involved in the transport process is very small. In fact the number of electrons occupying the extended (3D-like) states is several orders of magnitude smaller than that relative to the localized (2D-like) ones. This is basically due to the large energy separation (compared to the thermal energy) between localized states and the 3D continuum. From the point of view of the MC simulation, this implies that, in order to have a reasonably high number of transport electrons, one would need to simulate a huge number of particles. To overcome this problem, we have modified the simulation scheme presented above by implementing a weighted Monte Carlo (WMC) technique along the lines of Ref. 15. The basic idea of any weighted approach is to profit from the freedom of choice of the various probability distributions involved in the simulation process, e.g., initial carrier distribution, scattering rates, etc. This allows us to devote a large part of the simulation resources to a specific phase-space region of interest, namely, the energy range involved in transport processes. The specific WMC technique employed in our ''simulated experiments'' is summarized in Appendix B.

## III. NUMERICAL RESULTS

In this section we present our ''simulated experiments'' of vertical transport for two different MQW's. We start with a description of the computed band structures and then describe intraminiband and interminiband scattering rates due to LO phonons. The analysis of our simulated experiments starts with a discussion of the quasiequilibrium-response regime. In this case the validity of the proposed Monte Carlo (MC) approach is demonstrated by comparing our numerical simulations with available experimental data.[8] Finally, we discuss the hot-carrier transport regime. More specifically, we show how the phonon-induced scattering between extended and localized states can play a significant role in modifying the carrier mobility as well as the fraction of electrons involved in the vertical-transport process.

### A. Carrier band structure

The single-particle Schrödinger equation—which may include a self-consistent potential term—is solved using the plane-wave expansion presented in Appendix A. In Figs. 1(a) and 1(b) we plot the calculated band structures relative to two different potential profiles of interest for the present work.

(a) An $Al_{0.34}Ga_{0.66}As/GaAs$ (Ref. 25) MQW heterostructure, with undoped barriers of width $L_B=300$ Å and wells of width $L_W=45$ Å doped $n=1\times10^{17}$ cm$^{-3}$;

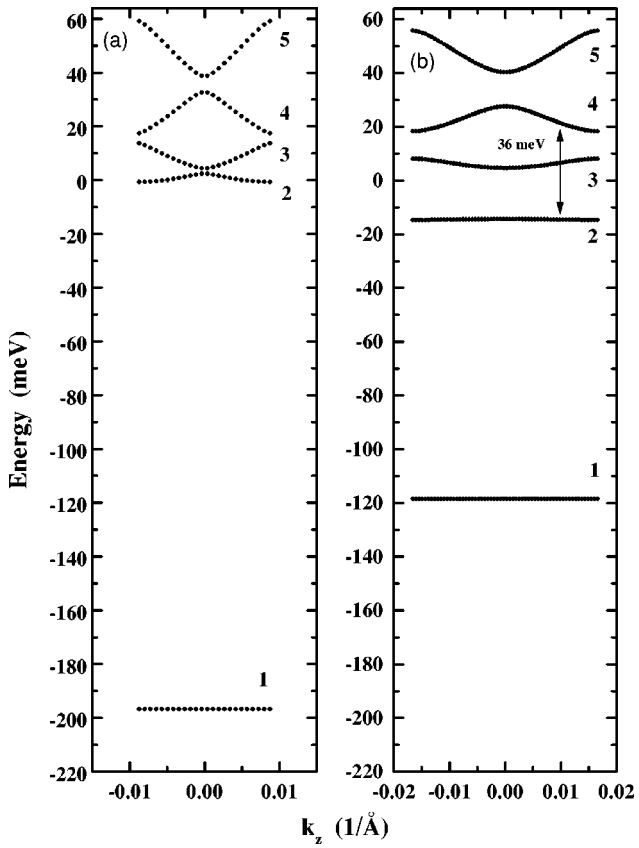


FIG. 1. Calculated band structures for (a) an $Al_{0.34}Ga_{0.66}As/GaAs$ multiple-quantum well (MQW) heterostructure, with $L_B=300$ Å and $L_W=45$ Å (barriers are undoped, and wells are doped $n=1\times10^{17}$ cm$^{-3}$); and (b) an $Al_{0.2}Ga_{0.8}As/GaAs$ MQW with $L_B=300$ Å and $L_W=73$ Å (GaAs layers are doped $n=1\times10^{17}$ cm$^{-3}$).

(b) An $Al_{0.2}Ga_{0.8}As/GaAs$ MQW with $L_B=300$ Å, and $L_W=73$ Å. GaAs layers are doped $n=1\times10^{17}$ cm$^{-3}$.

In Fig. 1 the different *Brillouin*-zone widths are due to different real-space periodicities. These are equal to $L_z=L_W+L_B=345$ and 373 Å for MQW's (a) and (b), respectively. To perform these band-structure calculations for each $k_z$ in the first *Brillouin* minizone a set of about 300 plane waves [see Eq. (A4)] was used. This is by far sufficient to describe accurately the energy range of interest.

### B. Carrier-phonon scattering rates

One of the main objectives of our MC analysis is to obtain a deeper insight in the interplay between delocalized (3D) and localized (2D) states mediated by electron-phonon interaction. These effects can be greatly amplified if we choose a band structure like the one reported in Fig. 1(b), where the interminiband transition $4\rightarrow2$ is resonant with the optical-phonon energy (i.e., 36 meV). An electron initially at the bottom of miniband 4 can be accelerated by the external electric field, and reach a region where the phonon emission rate is particularly strong owing to low momentum transfer. Indeed, for $\mathbf{k}_\parallel=0$ an abrupt change in the optical-phonon emission rate from miniband 4 to bound subband 2 is found as the threshold for emission is reached (at room temperature we obtain a jump from 0 to $\sim4$ ps$^{-1}$).

Figure 2 shows (continuous line) the total calculated emission and absorption room-temperature scattering rates from miniband 3 [panel (a)] and subband 1 [panel (b)] as a function of in-plane energy (the $k_z$ wave vector is fixed at the minizone center). For comparison we also show the scattering rates for transitions involving as final states bound subbands 1 and 2 only (dashed lines), i.e., transitions $3\rightarrow1,2$ [panel (a)] and $1\rightarrow1,2$ [panel (b)]. In Fig. 2(a) one can

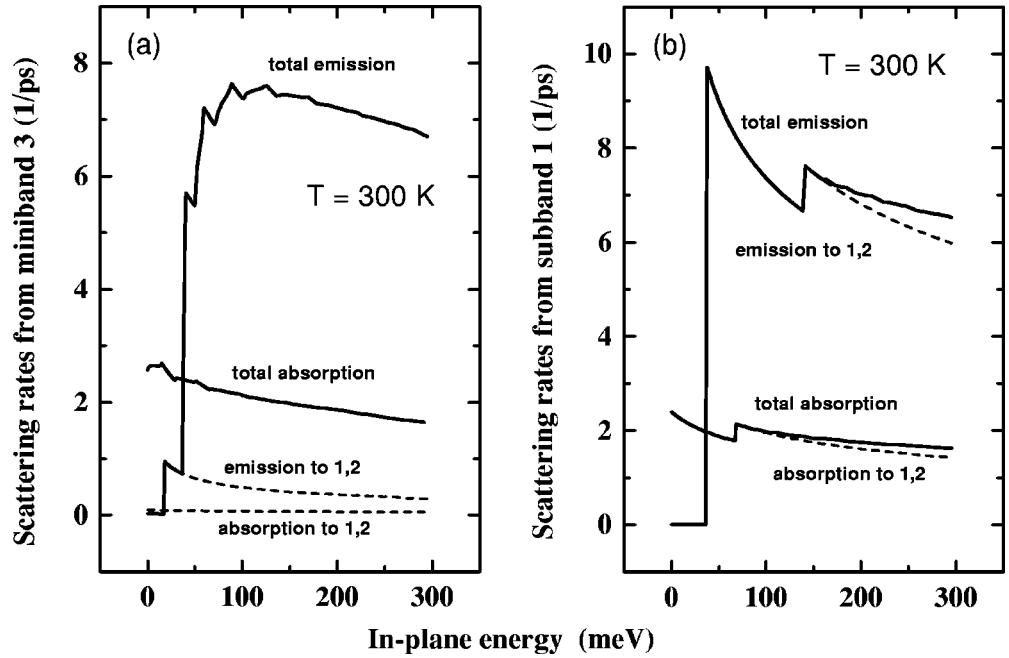


FIG. 2. Continuous line: total emission and absorption room-temperature scattering rates for the structure of Fig. 1(b) for $k_z=0$. All rates are plotted as a function of the in-plane energy. (a) Rates from miniband 3 and (b) rates from subband 1. Dashed line: emission and absorption room-temperature scattering rates from (a) miniband 3 and (b) from subband 1, to bound subbands 1 and 2 only.

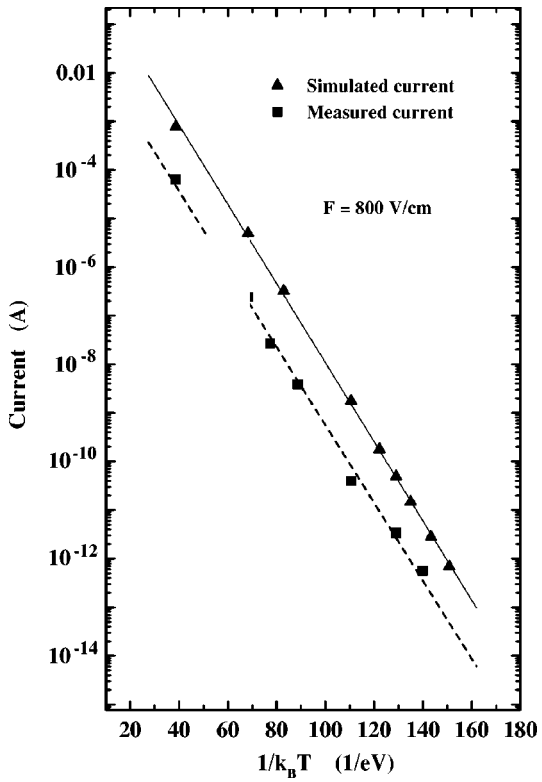


FIG. 3. Simulated current vs $1/k_BT$ in the 77–300 K temperature range for experimental and simulation data. Experimental data are taken from Ref. 8.

clearly see the steep change of the scattering rate as the in-plane energy reaches the threshold for transition into bound state 2 by phonon emission.[26]

The effect of the envelope-function overlap [see Eq. (10)] in determining transition probabilities is particularly evident for $3\rightarrow1$ and $1\rightarrow2$ emission. In Fig. 2(a) at low energies the emission rate is virtually zero owing to the fact that $\phi_{k_z3}$ has a strong antiresonance in the well region while the bound state 1 is strongly confined. After the threshold for emission into bound state 2 is reached $1\rightarrow2$ coupling [Fig. 2(b)], instead, produces a jump in the emission rate of $\sim1$ ps$^{-1}$ due to the strong overlap between wave functions $\phi_{k_z2}$ and $\phi_{k_z1}$. Finally, it should be underlined that the sharp peaks visible in Fig. 2(a) occur every time the threshold for emission (or absorption) in a new miniband is reached.

### C. Quasiequilibrium regime

Thermionic-emission current in MQW heterostructures has been widely studied since the end of the 1980s owing to its role in determining the ''dark current'' in MQW infrared photodetectors.[6–8,17–19] In this section we shall demonstrate that the present MC simulation approach can accurately reproduce the experimental thermionic-current temperature dependence. To this end, a comparison will be presented between simulations and experimental data available for the MQW heterostructure of Ref. 8.

In Fig. 3 we show a plot of the experimental current ($I$) vs $1/k_BT$ (squares) relative to the mentioned $Al_xGa_{1-x}As/GaAs$ MQW structure with an $x=0.3$ nominal aluminum concentration (see Ref. 8 for details). Here data shown correspond to an applied bias yielding a potential drop per period of 2.5 meV and an electric-field strength $F=800$ V/cm. The data exhibit a linear behavior with slope $S_{\rm exp}=-80$ meV (dashed line in Fig. 3). The slope value is particularly important because it is often used to determine the confinement barrier height by comparison to some appropriate analytical model.

In the same figure we also report the values of the simulated current obtained for the $Al_xGa_{1-x}As/GaAs$ MQW with $x=0.34$ [see Fig. 1(a)] corresponding to a conduction-band discontinuity of 285 meV (triangles).[25] We observe that the experimental linear behavior is successfully reproduced by our simulation (the solid line in Fig. 3). The given discontinuity (i.e., barrier composition) yields a slope $S_{sim}=-80.5$ meV in agreement with the experimental slope value. The fact that, for a fixed $T$, the simulated current is higher than the measured one can be linked to a difference between the nominal doping of the QWs ($n=1\times10^{17}$ cm$^{-3}$) and the effective one. Moreover, the effect of interface roughness (not considered here) could also lead to a decrease of the electron mobility without changing significantly its temperature dependence. Here, however, we want to stress that our MC simulation reproduces the correct current variation with temperature, yielding an *all-numerical* determination of the slope $S$ as well as of the conduction-band discontinuity without the need of an approximate analytical model.

Indeed, this fact could be used to determine which analytical expression best reproduces the actual barrier value. To this end it is useful to analyze the temperature dependence of the electron mean velocity in the continuum. This is shown in Fig. 4(a) for the same $F=800$ V/cm applied field: in contrast to the large current change [about nine orders of magnitude; see Fig. 4(b)], here we find a variation of less than one order of magnitude. Furthermore, as expected, we observe a *decrease* of electron mean velocity as a function of temperature due to enhanced scattering with optical phonons. The temperature dependence for the calculated drift velocity $\langle v\rangle$ is well described by

$$\langle v\rangle=2.5\times10^7-(6.9\times10^4)T\left(\frac{\rm cm}{\rm s}\right). \tag{24}$$

From this we deduce that by restricting the thermionic analysis to a temperature span of few tens of K, the assumption of a drift velocity independent of $T$ is a good approximation (within a few percent error).

These results support the modeling of thermionic-emission current by use of the simple expression[7,18,27]

$$I=en_e(T)v_0[1-e^{-eV_p/k_BT}], \tag{25}$$

where $e$ is the electron charge, $n_e(T)$ the density of 3D (propagating) electrons, $v_0=2.5\times10^7$ cm/s the characteristic drift velocity, and $V_p$ the average potential drop per period. The charge density $n_e(T)$ is proportional to $T^{3/2}e^{[\varphi-\mu(T)]/k_BT}$, where $\mu(T)$ and $\varphi$ are the chemical potential and the confining potential, (i.e., the energy difference between the onset of the continuum and the bound-state energy). From Eq. (25) we finally obtain

$$I\propto T^{3/2}e^{-[\varphi-\mu(T)]/k_BT}(1-e^{-eV_p/k_BT}). \tag{26}$$

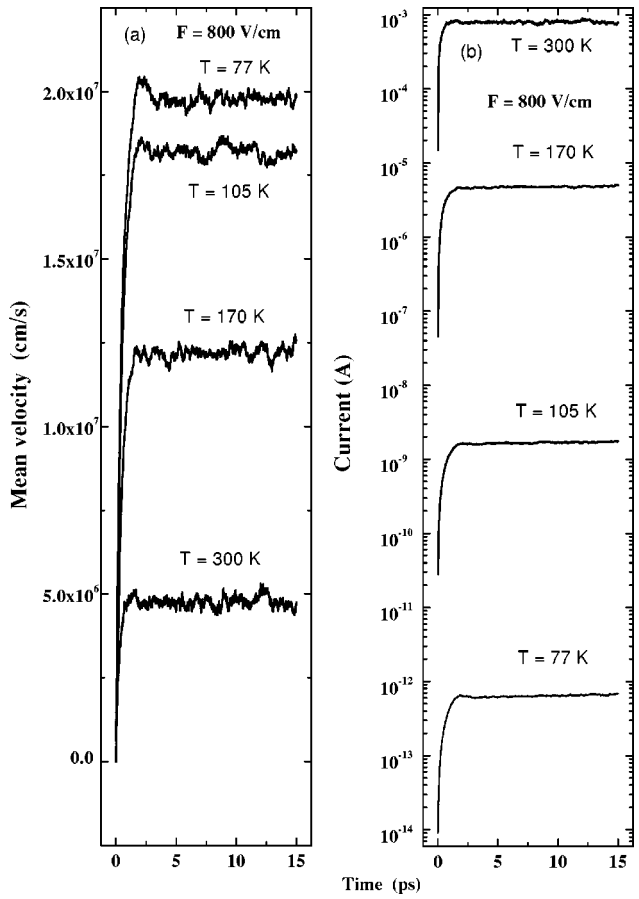


FIG. 4. $Al_{0.34}Ga_{0.66}As/GaAs$ heterostructure of Fig. 1(a). (a) Simulated mean velocity and (b) simulated current as a function of time in the 77–300-K temperature range for $F=800$ V/cm.

By using this expression to fit the calculated temperature dependence of the thermionic current in Fig. 3, we obtain $\varphi=199$ meV, in excellent agreement with the value actually used in the MC simulations ($\varphi=197$ meV).

A number of analytical models[17–19] have been used in the literature to provide a simple fitting procedure for the thermionic-emission data and to obtain the value for the confining potential. For low fields and low transmission barriers Eq. (26) is probably the most suitable for appropriately narrow temperature ranges; however, similar expressions have been used in the past with different values for the exponent $\alpha$ in the first $T^{\alpha}$ factor ($\alpha=1,\frac{3}{2},2$).[17–19] Starting from the same MC data discussed above, we obtained $\varphi=203$, 199, and 187 meV for $\alpha=1$, $\frac{3}{2}$, and 2, respectively. Indeed, such discrepancies are in most cases within experimental errors.

### D. Hot-carrier regime

In this section we shall examine in some detail the problem of carrier capture by QW's in MQW heterostructures in the presence of an external static electric field applied along the growth direction. Carrier-capture lifetimes are dominated by optical-phonon emission,[3] and most theoretical studies deal with this single scattering mechanism (capture mediated by impurities and carrier-carrier scattering was also considered[28–30]). Numerical calculations predict capture lifetimes $0.5\lesssim\tau_C\lesssim 2$ ps depending on carrier temperature and QW thickness. These values, as well as an oscillatory dependence on QW thickness, are in substantial agreement with experimental results which are obtained from time-resolved photoluminescence spectroscopy.[31,32] Conversely, a study of electron-capture processes in MQW's in the presence of a static driving electric field still remains a controversial subject because of its great complexity.[11,12] This is an important issue, however, and can have significant implications for the operation of MQW infrared detectors[6] as well as intersubband QW lasers.[33]

As discussed in Sec. III B, in order to emphasize carrier-phonon coupling between 3D and 2D states we have studied the $Al_{0.2}Ga_{0.8}As/GaAs$ heterostructure whose band structure is reported in Fig. 1(b). Figure 5 shows the time dependence of the simulated current $I$ and mean velocity $\langle v\rangle$ at $T=77$ K for two driving electric fields, namely, $F=500$ and 3000 V/cm. These two quantities are calculated according to

$$I=eS\sum_{\mathbf{k}\nu} f(\mathcal{E}_{\mathbf{k}\nu})v_{\nu}^{g}(k_z) \tag{27}$$

and

$$\langle v\rangle=\frac{\sum_{\mathbf{k}\nu\geqslant 3} f(\mathcal{E}_{\mathbf{k}\nu})v_{\nu}^{g}(k_z)}{\sum_{\mathbf{k}\nu\geqslant 3} f(\mathcal{E}_{\mathbf{k}\nu})}, \tag{28}$$

where

$$v_{\nu}^{g}(k_z)=\frac{1}{\hbar}\frac{\partial\epsilon_{\nu}(k_z)}{\partial k_z} \tag{29}$$

is the carrier group velocity ($v^g$ is equal to zero for dispersionless subbands 1 and 2). Here, $S$ is the structure cross section (perpendicular to the growth axis), and $f$ is the Fermi-Dirac distribution function. Velocity and current overshoots in Fig. 5 are linked to the fact that carriers accelerated by the electric field increase their energy in the continuum minibands, finally exceeding threshold for phonon emission by continuum→continuum and continuum→bound-subband 2 transitions. Note that Eqs. (27) and (28) clearly show that as long as no carriers transfer between 3D and 2D states, any relative current variation $\Delta I/I$ will be equal to $\Delta\langle v\rangle/\langle v\rangle$. For both field intensities examined, however, we find that relative current overshoots are greater than the corresponding velocity ones. This suggests that carriers have transferred from 3D to 2D bound states. For $F=3000$ V/cm the effect is much more pronounced, denoting a marked field dependence. Carrier trapping can be directly seen by inspecting Fig. 6, where we report the relative population variations during the first several ps for the same field intensities (here $N^3$, $N^{3+}$, and $N^{4+}$ denote carrier populations of minibands with indices $\nu=3$, $\nu\geqslant 3$, and $\nu\geqslant 4$, respectively). After a small increase, population of the continuum ($N^{3+}$, solid line in Fig. 6) indeed exhibits a strong decrease to less than half its initial value. The field dependence of this effect is shown in Fig. 7, where relative $N^{3+}$ and $N^{4+}$ variations at different fields are displayed. For very low field intensities ($F\lesssim 10$ V/cm), the fraction of carriers in the continuum slightly increases: the carrier mean kinetic energy is not suf-

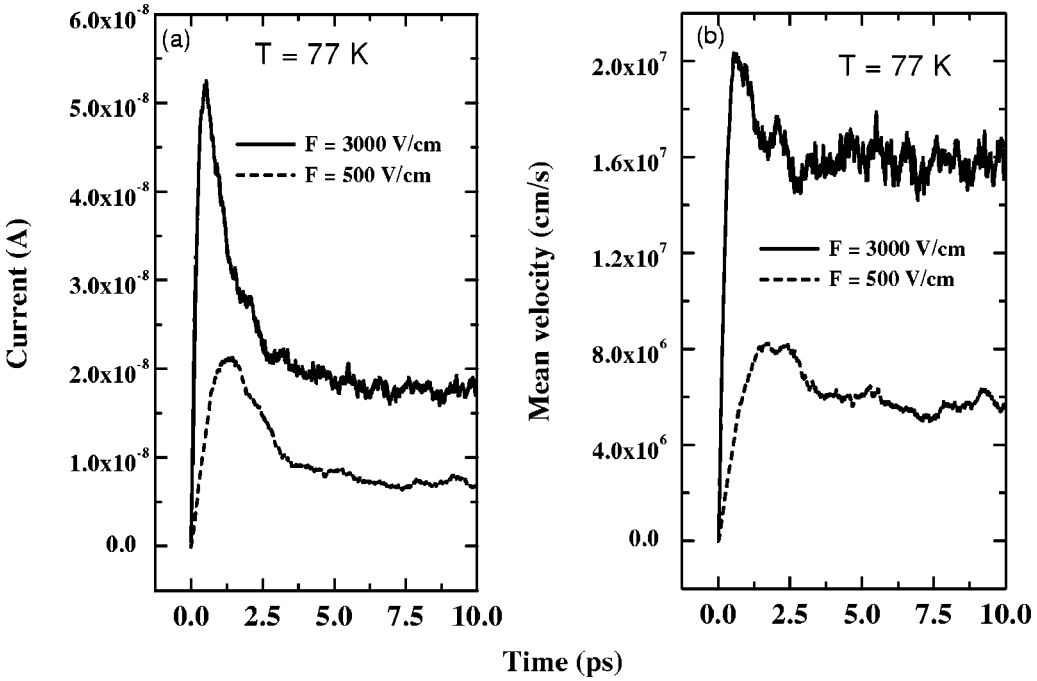


FIG. 5. Heterostructure of Fig. 1(b). Time dependence of simulated current (a) and mean velocity (b) at 77 K. Two different applied fields are considered: $F=500$ and 3000 V/cm.

ficiently high to reach the threshold for scattering into subband 2. At higher fields we observe an increasing carrier trapping in the QW, saturating in the region $F \gtrsim 800$ V/cm. The temperature dependence of this carrier-capture process is illustrated by Fig. 8 for the case $F=800$ V/cm. Here, relative $N^{3+}$ and $N^{4+}$ variations are monitored in the 77–300-K temperature range. They display a suppression of population variation at increasing temperatures. This is expected since larger temperatures imply a larger number of populated minibands at equilibrium. One can give a condition for the onset of continuum depopulation effect as $N^{4+}/N^{3+} \ll 1$ at time $t=0$, i.e., $k_B T \ll 36$ meV.

## IV. CONCLUSIONS

In summary, we have proposed a microscopic approach for the analysis of vertical-transport phenomena in semiconductor heterostructures. By means of a fully three-

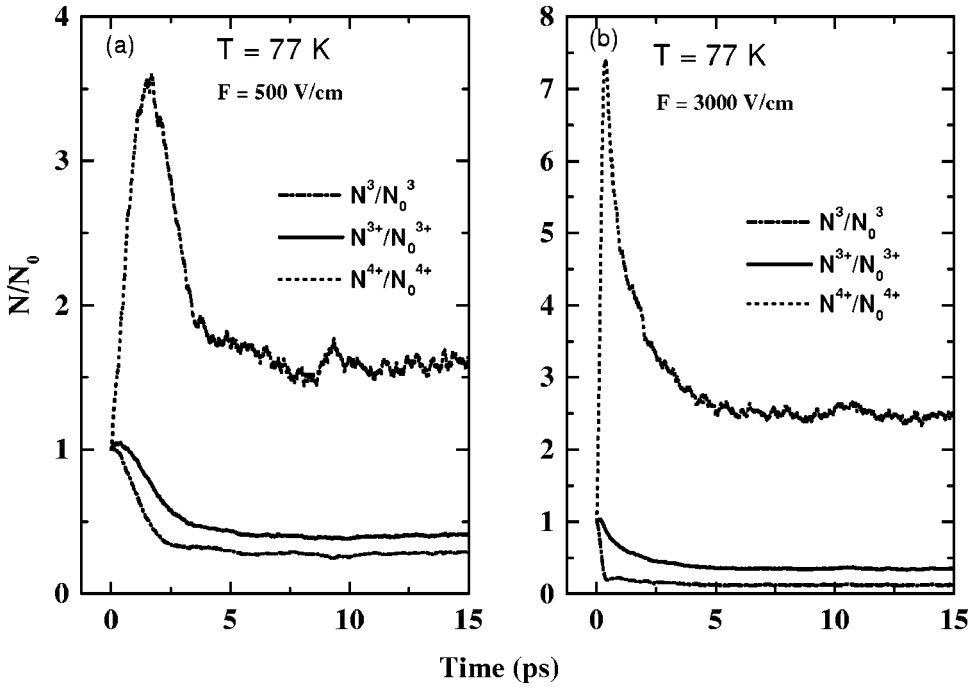


FIG. 6. Heterostructure of Fig. 1(b). Time variation of the carrier population for $F=500$ V/cm (a) and $F=3000$ V/cm (b). $N^3$, $N^{3+}$, and $N^{4+}$ denote carrier population of minibands with $\nu=3$, $\nu \geqslant 3$, and $\nu \geqslant 4$, respectively. Populations at $t=0$ are labeled $N_0$. $T=77$ K.

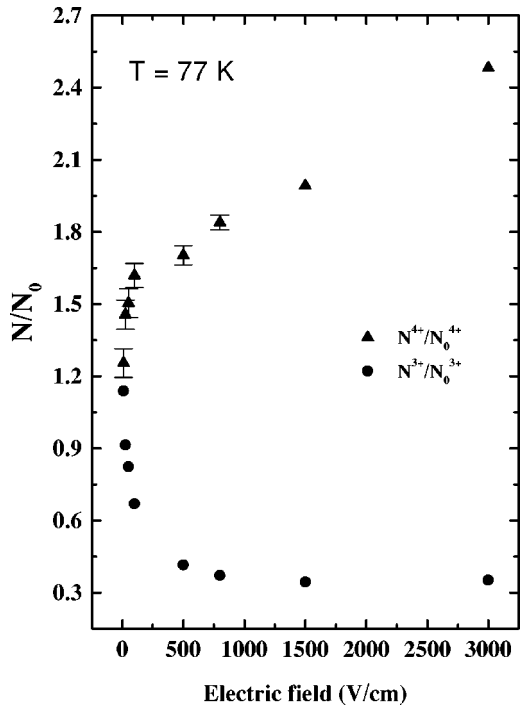


FIG. 7. Heterostructure of Fig. 1(b). Steady-state relative population variations for different electric-field intensities. Here $N_0^{3+}$ and $N_0^{4+}$ denote population at time $t=0$.

dimensional description of carrier wave functions and energy bands, all relevant electron-phonon scattering rates for both intraminiband and interminiband transitions have been considered. This has allowed a quantitative evaluation of scattering-induced coupling between extended (3D-like) and localized (2D-like) states in hot-carrier transport across a generic heterostructure.

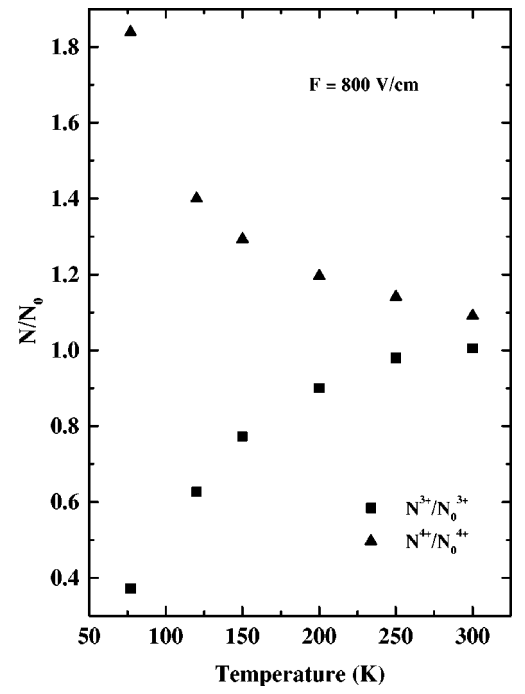


FIG. 8. Temperature dependence of relative population variations for $F=800$ V/cm.

The proposed MC simulation scheme has been applied to finite MQW's with different geometries. A detailed analysis of the electron current as a function of temperature shows good agreement with experiments. Moreover, our analysis of the electron current through the heterostructure shows the role played by phonon-induced transitions between extended and localized states. In particular, in addition to a reduction of the carrier mobility, a field-induced suppression of the number of ''conducting carriers'' is found to take place. For a better understanding of this phenomenon, an *ad hoc* quantum structure—characterized by a strong scattering coupling between high-energy conduction states and localized states—has been considered. Although we do not believe that this depopulation effect could be easily probed experimentally, we nevertheless think that our simulations results could be of help in optimizing the design of MQW infrared detectors.

## ACKNOWLEDGMENTS

We are grateful to Guido Goldoni and Elisa Molinari for stimulating and fruitful discussions. This work was supported in part by the European Commission through the TMR Network ''Ultrafast Quantum Optoelectronics'' and Brite-Euram UNISEL project (Contract No. BE97-4072).

## APPENDIX A: SELF-CONSISTENT SCHRÖDINGER-POISSON CALCULATION OF SINGLE-PARTICLE STATES

In this section we shall discuss the numerical approach used for the self-consistent calculation of the carrier wave functions in a generic heterostructure. To this end, let us recall the explicit form of the 1D Schrödinger equation for the envelope function $\phi_{k_z}(z)$:

$$\left[-\frac{\partial}{\partial z}\left(\gamma(z)\frac{\partial}{\partial z}\right)+V(z)\right]\phi_{k_z\nu}(z)=\epsilon_{k_z\nu}\phi_{k_z\nu}(z), \quad \text{(A1)}$$

with $\gamma(z)=\hbar^2/2m(z)$. Here $V(z)=V_0(z)+\Delta V(z)$ includes both the heterostructure potential profile $V_0$ and the internal potential $\Delta V$, which in turn is obtained by solving the Poisson equation

$$\frac{\partial^2}{\partial^2 z}\Delta V(z)=-\frac{\rho(z)}{\varepsilon}. \quad \text{(A2)}$$

Here $\rho(z)=\rho_0(z)+\Delta\rho(z)$ is the sum of the fixed charge density $\rho_0$ (due to the particular doping profile) and of the free charge

$$\Delta\rho(z)=e\sum_{\mathbf{k}\nu} f(\mathcal{E}_{\mathbf{k}\nu})|\phi_{k_z\nu}(z)|^2, \quad \text{(A3)}$$

where $f$ denotes the Fermi-Dirac distribution function.

Our aim is to perform a self-consistent solution of Eqs. (A1) and (A2). Contrary to the conventional methods based on real-space finite-difference schemes, the proposed approach is based on a plane-wave expansion of both equations.

Let us consider the following set of basis wave functions:

$$\chi_{k_z,G}(z)=\frac{1}{\sqrt{L_z}}e^{i(G+k_z)z}, \tag{A4}$$

where $L_z$ denotes the periodicity interval along the $z$ direction, $G_n=2\pi n/L_z$ are the corresponding reciprocal-lattice vectors ($n=0,\pm1,\pm2,\ldots$), and $k_z$ is the quasimomentum limited to the first Brillouin zone ($-\pi/L_z\leqslant k_z\leqslant\pi/L_z$).

Since the above basis functions $\chi$ obey the same boundary conditions as the wave functions $\phi$ in Eq. (3), the latter can be expanded over the reciprocal-lattice vectors $G$ according to

$$\phi_{k_z}(z)=\sum_G c_{k_z,G}\chi_{k_z,G}(z). \tag{A5}$$

By inserting the above plane-wave expansion into Eqs. (A1) and (A2), we obtain the following set of coupled equations:

$$\sum_{G'}(H_{k_z,GG'}-\epsilon_{k_z}\delta_{GG'})c_{k_z,G'}=0,$$

$$G^2\overline{\Delta V}_G=\frac{e}{\varepsilon}\sum_{\mathbf{k}\nu}f(\mathcal{E}_{\mathbf{k}\nu})\sum_{G'}c^*_{k_z,G'}c_{k_z,G+G'}, \tag{A6}$$

with

$$H_{k_z,GG'}=(k_z+G)\overline{\gamma}_{G-G'}(k_z+G')+\overline{V}_{G-G'}. \tag{A7}$$

The bar indicates Fourier transforms with respect to our reciprocal-lattice vectors, i.e.,

$$\overline{A}_G=\frac{1}{\sqrt{L_z}}\int_{-L_z/2}^{+L_z/2}e^{-iGz}A(z). \tag{A8}$$

The system of coupled equations (A6) consists of an eigenvalue problem (which provides carrier energies and wavefunctions) plus an algebraic version of the Poisson equation. They are solved by means of the following iterative procedure. As an initial condition, we evaluate the carrier eigenstates by solving the eigenvalue problem in the absence of internal potential, i.e., we take $\overline{\Delta V}=0\rightarrow\overline{V}=\overline{V}_0$. The resulting zero-order eigensolutions (i.e., energy bands $\epsilon_{k_z}$ and wave-function coefficients $\{c_{k_z,G}\}$) are then inserted into the Poisson equation which, in turn, provides the first-order internal potential $\overline{\Delta V}$. The above two-step procedure is repeated until convergence is achieved.

For the typical heterostructures considered in this paper, we have used a set of about 300 plane waves with a period of about 50 nm. This allows us to obtain with great accuracy the wave functions and miniband dispersions corresponding to the confined (2D-like) states. However, for a detailed analysis of continuum states (3D-like) convergence problems may arise for two reasons: first, the number of plane waves may be inadequate; and second, a fictitious coupling due to the finite dimensions of our periodicity box may play some role. By increasing the number of plane waves and the size of the box, we have checked that this is definitely not the case for the ''close-to-gap'' energy region discussed in this paper.

## APPENDIX B: WEIGHTED MONTE CARLO (WMC) PROCEDURE

In this section we shall briefly discuss the specific WMC approach used in our simulated experiments. As anticipated in Sec. II C, the aim of any weighted approach is to profit from the freedom of choice of the various probability distributions involved in the simulation process, e.g., initial carrier distribution, scattering rates, etc. This allows us to devote a large part of the simulation resources to a specific phase-space region of interest, which in our case coincides with the energy range involved in the vertical-transport process. A general discussion of the WMC method, including some applications to semiclassical as well as quantum-transport problems, can be found in Ref. 15 and will not be repeated here. Instead, we will briefly describe the specific nature of our weighted simulation scheme.

To this end, let us rewrite the set of Boltzmann-like equations (18) as

$$\frac{\partial}{\partial t}f_{\mathbf{k}\nu}+\frac{e\mathbf{F}}{\hbar}\cdot\nabla_{\mathbf{k}}f_{\mathbf{k}\nu}=-\Gamma_{\mathbf{k}\nu}f_{\mathbf{k}\nu}+\sum_{\mathbf{k}'\nu'}P_{\mathbf{k}\nu,\mathbf{k}'\nu'}f_{\mathbf{k}'\nu'}, \tag{B1}$$

where

$$\Gamma_{\mathbf{k}\nu}=\sum_{\mathbf{k}'\nu'}P_{\mathbf{k}'\nu',\mathbf{k}\nu} \tag{B2}$$

is the total scattering rate for intraminiband and interminiband processes. As described in Ref. 15, the MC method provides a statistical sampling of the various distribution functions $f_{\mathbf{k}\nu}$ through a random generation of free flights and scattering events. More specifically, the total scattering rate $\Gamma_{\mathbf{k}\nu}$ (which can be regarded as the semiclassical lifetime of state $\mathbf{k}\nu$) determines the free-flight duration, while the probabilities $P_{\mathbf{k}\nu,\mathbf{k}'\nu'}$ determine the carrier state after scattering.

Let us now consider a generic probability distribution $W_\nu$ as a function of the miniband index $\nu$ only: $0<W_\nu<1$ and $\Sigma_\nu W_\nu=1$. Starting from such distribution we introduce a weighted carrier distribution function $f^W$ according to

$$f^W_{\mathbf{k}\nu}=W_\nu f_{\mathbf{k}\nu}. \tag{B3}$$

We can then rewrite the set of Boltzmann-like equations in Eq. (B1) as

$$\frac{\partial}{\partial t}f^W_{\mathbf{k}\nu}+\frac{e\mathbf{F}}{\hbar}\cdot\nabla_{\mathbf{k}}f^W_{\mathbf{k}\nu}=-\Gamma^W_{\mathbf{k}\nu}f^W_{\mathbf{k}\nu}+\sum_{\mathbf{k}'\nu'}P^W_{\mathbf{k}\nu,\mathbf{k}'\nu'}f^W_{\mathbf{k}'\nu'}, \tag{B4}$$

with

$$\Gamma^W_{\mathbf{k}\nu}=\Gamma_{\mathbf{k}\nu},\quad P^W_{\mathbf{k}\nu,\mathbf{k}'\nu'}=\frac{W_\nu}{W_{\nu'}}P_{\mathbf{k}\nu,\mathbf{k}'\nu'}. \tag{B5}$$

As we can see, Eq. (B4) has exactly the same form of the original Boltzmann-like equation (B1); therefore it is still suitable for a MC solution, provided we replace the original rates with the weighted ones [Eqs. (B5)]. Such a weighted approach can be regarded as a proper phase transformation over the miniband index $\nu$, which leads to a fictitious modification of the carrier density of states.

Since our aim was to devote a significant fraction of simulated carriers to the continuum (transport) energy region, we have artificially reduced the statistical weight of the minibands corresponding to bound states. More specifically, we have chosen the distribution probability

$$W_\nu = \frac{e^{E_\nu/k_BT}}{\sum_\nu e^{E_\nu/k_BT}}, \tag{B6}$$

with

$$E_\nu = \begin{cases} \epsilon_{\mathbf{0}\nu} & \text{for bound-state minibands} \\ 0 & \text{for continuum-state minibands} \end{cases} \tag{B7}$$

[here $\epsilon_{\mathbf{0}\nu}$ denotes the carrier energy in miniband $\nu$ at the center of the Brillouin zone ($\mathbf{k}=\mathbf{0}$)]. The above probability distribution allows us to increase the fraction of simulated carriers in the continuum by several orders of magnitude, thus strongly reducing the statistical fluctuations in the stochastic evaluation of $f^W_{\mathbf{k}\nu}$. Given such fictitious carrier distribution—obtained as a result of the above weighted MC approach—any single-particle physical quantity $A$, e.g., charge current, mean kinetic energy, etc., is evaluated according to

$$\langle A \rangle = \sum_{\mathbf{k}\nu} A_{\mathbf{k}\nu} f_{\mathbf{k}\nu} = \sum_{\mathbf{k}\nu} A_{\mathbf{k}\nu} \frac{f^W_{\mathbf{k}\nu}}{W_\nu}. \tag{B8}$$


[1] L. Esaki and R. Tsu, IBM J. Res. Dev. **14**, 61 (1970).

[2] *Physics of Quantum Electron Devices*, edited by F. Capasso (Springer, Berlin, 1990).

[3] J. Shah, in *Ultrafast Spectroscopy of Semiconductors and Semiconductor Nanostructures*, edited by M. Cardona, P. Fulde, K. von Klitzing, and H. J. Queisser (Springer, Berlin, 1996).

[4] *Theory of Transport Properties of Semiconductor Nanostructures*, edited by E. Schöll (Chapman & Hall, London, 1998).

[5] F. Capasso, W.T. Tsang, G.F. Williams, IEEE Trans. Electron Devices **ED-30**, 381 (1983).

[6] B.F. Levine, J. Appl. Phys. **74**, R1 (1993).

[7] *Semiconductor Quantum Wells and Superlattices for Long-Wavelength Infrared Detectors*, edited by M. O. Manasreh (Artech House, Boston, 1993).

[8] S. Barbieri, F. Mango, F. Beltram, M. Lazzarino, and L. Sorba, Appl. Phys. Lett. **67**, 250 (1995).

[9] S. Barbieri, F. Mango, F. Beltram, M. Lazzarino, and L. Sorba, Superlattices Microstruct. **23**, 1079 (1998).

[10] H. C. Liu, A. G. Steele, M. Buchanan, and Z. R. Wasilewski, in *Intersubband Transitions in Quantum Wells*, edited by E. Rosancher, B. Vinter, and B. F. Levine (Plenum, New York, 1992), p. 57.

[11] E. Rosancher, B. Vinter, F. Luc, L. Thibaudeau, P. Bois, and J. Nagle, IEEE Trans. Quantum Electron. **30**(12), 2875 (1994).

[12] L. Thibaudeau, P. Bois, and J.Y. Duboz, J. Appl. Phys. **79**, 446 (1996).

[13] C. Jacoboni and P. Lugli, *The Monte Carlo Method for Semiconductor Device Simulations* (Springer, Vienna, 1989).

[14] S.M. Goodnick and P. Lugli, in *Hot Carriers in Semiconductor Nanostructures: Physics and Applications*, edited by J. Shah (Academic, San Diego, 1992), p. 191.

[15] F. Rossi, P. Poli, and C. Jacoboni, Semicond. Sci. Technol. **7**, 1017 (1992).

[16] F. Rossi, T. Meier, P. Thomas, S.W. Koch, P.E. Selbmann, and E. Molinari, Phys. Rev. B **51**, 16 943 (1995).

[17] S.R. Andrews and B.A. Miller, J. Appl. Phys. **70**, 993 (1991).

[18] M. J. Kane, S. Millidge, M. T. Emeny, D. Lee, D. R. P. Guy, and C. R. Whitehouse, in *Intersubband Transitions in Quantum Wells*, edited by E. Rosancher, B. Vinter, and B. F. Levine (Plenum, New York, 1992), p. 31.

[19] E. Pelve, F. Beltram, C.G. Bethea, B.F. Levine, V.O. Shen, S.J. Hsieh, and R.R. Abbott, J. Appl. Phys. **66**, 5656 (1989).

[20] E. Molinari, in *Confined Electrons and Photons: New Physics and Applications*, edited by E. Burstein and C. Weisbuch (Plenum, New York, 1994).

[21] H. Rücker, E. Molinari, and P. Lugli, Phys. Rev. B **45**, 6747 (1992).

[22] T. Kuhn and F. Rossi, Phys. Rev. Lett. **69**, 977 (1992); Phys. Rev. B **46**, 7496 (1992).

[23] F. Rossi, Semicond. Sci. Technol. **13**, 147 (1998).

[24] W. Quade, E. Schöll, F. Rossi, and C. Jacoboni, Phys. Rev. B **50**, 7398 (1994).

[25] The aluminum concentration value $x$ was linked to the conduction-band discontinuity $\Delta E_c$ by the relation $\Delta E_c = x \times 0.827$ (eV).

[26] The maximum value of $\sim 1$ ps$^{-1}$ calculated in this case cannot be directly compared with the $\sim 4$ ps$^{-1}$ value obtained for the $4 \rightarrow 2$ rate. In fact these two transitions involve different initial minibands 3 and 4, respectively, with different envelope functions.

[27] B.F. Levine, C.G. Bethea, G. Hasnain, V.O. Shen, E. Pelve, R.R. Abbott, and S.J. Hsieh, Appl. Phys. Lett. **56**, 851 (1990).

[28] B. Deveaud, A. Chomette, D. Morris, and A. Regreny, Solid State Commun. **85**, 367 (1993).

[29] P.W.M. Blom, J. Claes, J.E.M. Haverkort, and J.H. Wolter, Opt. Quantum Electron. **26**, S667 (1994).

[30] P.J. van Hall and P.W.M. Blom, Superlattices Microstruct. **13**, 329 (1993).

[31] P.W.M. Blom, C. Smit, J.E.M. Haverkort, and J.H. Wolter, Phys. Rev. B **47**, 2072 (1993).

[32] M.R.X. Barros, P.C. Becker, D. Morris, B. Deveaud, A. Regreny, and F.A. Beisser, Phys. Rev. B **47**, 10 951 (1993).

[33] J. Faist, F. Capasso, D.L. Sivco, C. Sirtori, A.L. Hutchinson, and A.Y. Cho, Science **264**, 553 (1994).